A manual for Seagrass and seaweed beds distribution mapping with satellite images

Teruhisa Komatsu

Atmosphere and Ocean Research Institute
The University of Tokyo

March 2015

This manual is under peer review and subject to change.

Index

1. Introduction

In coastal waters, seagrass and seaweed beds (Figures 1 and 2) provide important ecological functions such as habitats for animals and plants, and stabilizing effects of environments such as buffering effect of currents and water movement, promotion of sedimentation, absorption of nutrients, production of oxygen, sediment retention, etc. (*e.g*. Komatsu, 1996; Komatsu, 1989; Komatsu and Yamano, 2000). Thus they contribute to marine biodiversity and also human society through ecological services (*e.g*. Costanza *et al*., 1997). They have been destroyed due to human impacts such as direct ones of fisheries and reclamation, indirect ones such as pollution through aquaculture and urban and industrial wastewaters during economic development (Komatsu, 1997).

In the Seto Inland Sea, fish culture such as yellowtail has been developed since 1960s. In Asia, aquaculture (*e.g*. shrimp and marine fish farming) has also been developed since 1970-80s (*e.g*. Guiji and Finger-Stich, 1996; Huitric *et al*., 2002). Aquacultures such as yellowtail and sea breams need a large quantity of live baits such as anchovy, sardine and mackerel. Cultured fish excrete a large quantity of feces and urine into water. Since cultured fish don't consume all fed bait, leftovers appear. These organic matters are decomposed by aerobic bacteria consuming oxygen in seawater. Nutrients produced from organic matters promote an increase in phytoplankton and generate harmful algal blooms. In such a phytoplankton rich environment, transparency is decreased. Eventually, lower depth limits of seagrass beds become shallower and seagrass beds are shrunk. On the sea bed, sediments become anaerobic condition and muddy due to accumulation of organic matter on the seabed and consumption of oxygen by aerobic bacteria decomposing organic matters. While repeat of fish culture for long time, feces, urine and leftovers of fish deteriorate water quality and bottom sediment quality, which is called as self pollution. Consequently, sandy bottom is changed to soft muddy bottom due to increase in thickness of anaerobic layer. The soft muddy bottom prevents seagrasses from rooting because they are easily taken off from the bottom by the waves and currents. This is also true for shrimp culture because discharge from shrimp ponds causes eutrophication and lead to destruction of seagrass and seaweed beds due to water quality deterioration (*e.g*. Dierberg and Kiattisimkul, 1996; Naylor *et al*., 2000).

Seagrass and seaweed beds, however, have to be conserved for marine biological diversity and sustainable development of fisheries and society. For maintaining sound seagrass and seaweed beds, it is necessary to monitor their present spatial distributions, and to establish databases and information networks to share and disseminate their data to manage these beds (Komatsu *et al*., 2002c). We can also analyze archived satellite images to know past seagrass and seaweed distributions. In this manual, we introduce a practical satellite remote sensing method specialized for mapping seagrass and seaweed beds including validation of satellite images by ground truthing.

Figure 1. Photo showing *Zostera caulescens* Miki in Funakoshi Bay, Iwate Prefecture, Japan

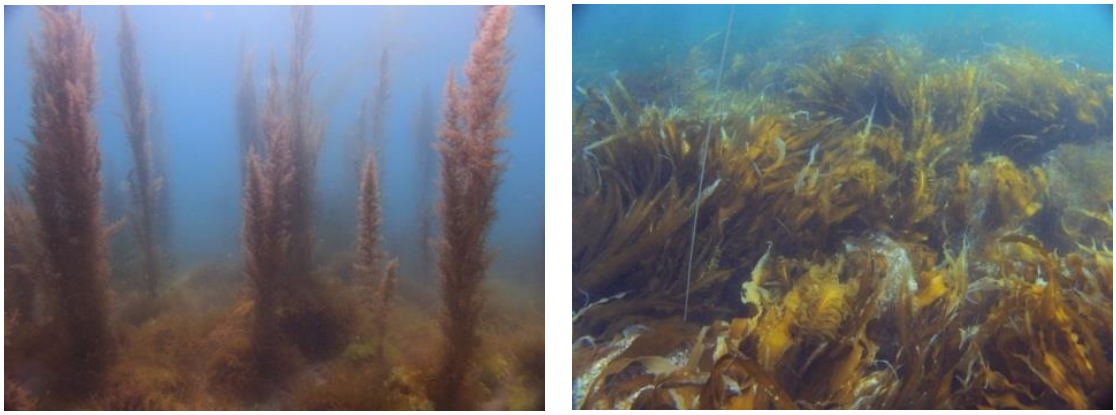

Figure 2. Photos showing forests of brown algae, *Stephanocystis hakodatensis* (Yendo) Draisma, Ballesteros, Rousseau et Thibaut (left photo), and *Saccharina japonica* (Areschoug) Lane, Mayes, Druehl et Saunders var. *religiosa* (Miyabe) Yotsukura, Kawashima, Kawai, Abe et Druehl (right photo) off Kamoenai, west coast of Hokkaido, Japan.

2. Optics for remote sensing

Light is one type of electromagnetic radiation, of which the true units are W m^{-2} sr^{-1} μm^{-1}, consisting of wide range of wave lengths. Although visible and near-infrared bands are generally available in satellite images, the visible bands can penetrate into the sea deeper than ultra-violet and near-infrared which are easily absorbed by the surface thin layer (Kawahara *et al*., 2000). Thus, visible bands are used for mapping habitats in coastal waters under the sea. In the ocean, a blue band and a red band reach the deepest and shallowest depths among blue, red and green bands, respectively (Figure 3).

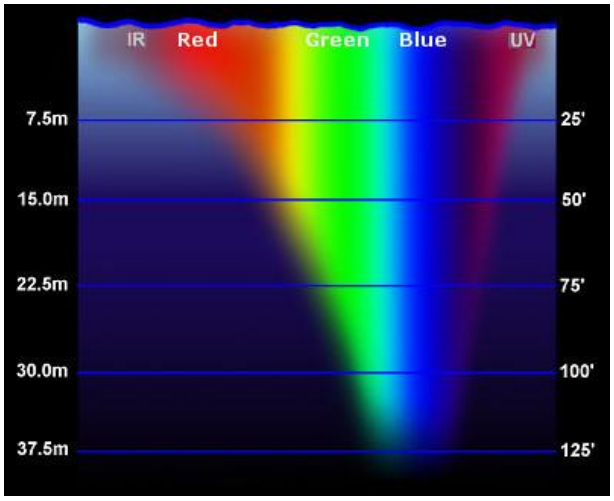

Figure 3. Patterns of vertical penetration of light between ultraviolet and infrared into the water (Source: http://www.seos-project.eu/modules/oceancolour/oceancolour-c01-p07.html)

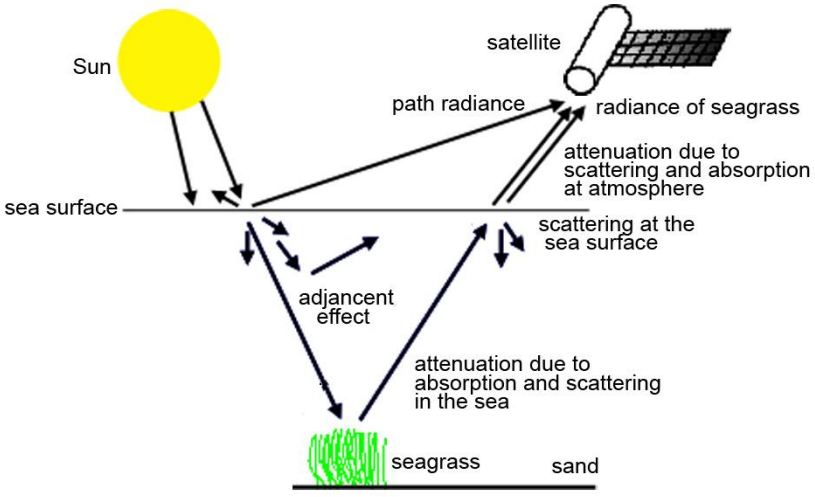

Figure 4. Schematic view of passage of electromagnetic radiation from the Sun to the satellite sensor

through atmospheric layer, sea water column and sea bottom surface.

Remote sensing by a satellite utilizes radiance of the visible bands from the sea beds received by an optical onboard sensor. The passage of visible band radiation from the sun to the satellite sensor is shown as a simplified schematic diagram in Figure 4. The visible band radiation from the sun passes two layers: atmosphere and water. In both layers, a part of light is absorbed and scattered by molecules and particulates from the sun to the sea bottom and from the sea bottom to the satellite. A part of light is also reflected by the sea surface. Radiances of visible bands recorded as digital numbers of pixels by the satellite sensor include bottom reflectance depending on substrate types (Figure 4). Thus, difference in reflectance of visible bands on the bottom surface under the shallow sea can be used to classify substrate types. In general, an optical sensor mounted on a satellite detects three bands of blue, green and red colors, while spectral distribution of each band depends on the optical sensor. Blue band is important to detect bottom types in deeper depth.

Reflectance is a ratio of leaving to incident radiation of a certain spectral window on surface of substrate. Figure 5 shows reflectance of sand and one species of Mediterranean seagrass, *Posidonia oceanica* L., from ultra-violet to infrared measured with a spectrometer (FieldSpec Pro, Analytical Spectral Devices Inc., USA) of which the instantaneous field of view was 25 degree. We put samples into a basin with a diameter of 30 cm, which was painted in black paint not to enter the light from surrounding environment into the basin. We measured radiances of the samples and a white disk around noon in a fine day without clouds from a wave length of 350 nm to 2500 nm at one nm intervals. Reflectance of a sample was calculated by dividing radiance of the sample with that of the white disk at each wave length. We can find the differences in reflectance of visible bands between them. Since sand reflects from short wave length to long wave length, its color is white. On the other hand, the seagrass reflects green band around 550 nm. Then its color is green. If differences in reflectances exist corresponding to spectral windows of satellite optical sensor, it is possible to distinguish substrate types.

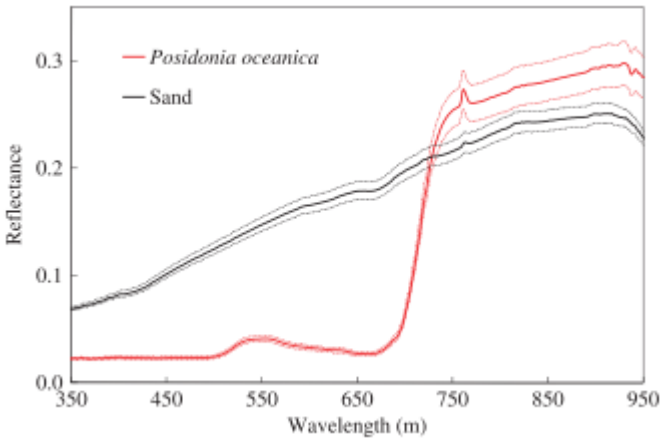

Figure 5. Reflectance level with reference to wavelength for each bottom feature (Mahares). Values (bold lines) are shown as the mean (±standard deviation represented by broken lines). For each bottom feature, n=5. (Source: Sagawa *et al.*, 2010)**3. Satellite images and software**

3. 1. Spatial, spectral and radiometric resolutions of satellite images

A multiband satellite image includes multiband data, which are generally composed of blue, green, red and near-infrared layers. Each layer consists of raster cells, pixels. One pixel corresponds to an area with intensity of upwelling radiation of this band through the area on the Earth surface. For mapping coastal habitats, the spatial resolution of satellite images must be finer than a habitat dimension. Thus, the most important thing for remote sensing of coastal habitats is that plural pixels more than five can cover an area of habitat to detect it. This relation is relative between spatial resolution of satellite and areas of habitats. In generally, seagrass and seaweed beds are distributed in a horizontal scale of several meters to hundred or thousand meters. World View 2/3, Geo Eye-1, Quick Bird-2, IKONOS, Pleiades-1/2, SPOT 6/7, LANDSAT 8 OLI, LANDSAT ETM+, ALOS AVNIR-2 have the spatial resolutions described in Table 1. They can detect marine habitat on the sea bottom greater than their own limits of habitat sizes. Images of World View 2/3, Geo Eye-1, Quick Bird-2, IKONOS and Pleiades-1/2 have very high spatial resolutions of pixel less than 4 m (Table 1).

Radiometric resolution is an ability of sensor to discriminate small differences in the magnitude of radiation within the ground area that corresponds to a single raster cell. When the bit depth (number of data bits per pixel) of the images that a sensor records is great, its radiometric resolution is high. Digital sensors of satellite record the intensity of electromagnetic radiation from each spot viewed on the Earth's surface as a digital number (DN) for each spectral band. The exact range of DN that a sensor utilizes depends on its radiometric resolution. The World View 2/3, Geo Eye-1, Quick Bird-2, IKONOS sensors, for example, have 11 bits (0-2047) per band per pixel and Pleiades-1/2 and LANDSAT 8 OLI have 12 bits (0-4094), while ALOS AVNIR 2 and LANDSAT ETM+ have 8 bits (0-255) (Table 1). Thus the first two groups of satellites can distinguish small differences in the magnitude of radiation among substrate types.

Spectral resolution is the ability of a sensor to detect small differences in wavelength. A panchromatic sensor is sensitive to a broad range of wavelengths. An object that reflects a lot of energy in the blue area of the visible band would be indistinguishable in a panchromatic photo from an object that reflected the same amount of energy in the red band. A sensing system with higher spectral resolution would make it easier to distinguish the two objects apart. Geo Eye-1, Quick Bird-2, IKONOS, Pleiades 1/2, SPOT 6/7 and ALOS AVNIR 2 have multiband sensors measuring blue, green, red and infrared bands while SPOT XS does green, red and infrared bands (Table 1). Their spectral resolutions are similar. World View 2 and 3 have coastal, blue, green, yellow, red and infrared bands. LANDSAT 8 OLI has coastal (new deep blue), blue, green, yellow, red and two infra red bands. Sensors with high spectral resolution are a hyper spectral sensor. Compact airborne hyper spectral bands (CASI) have been often used for mapping coral reef ecosystems. This system is very effective with high spatial and spectral resolutions for coastal mapping. However, their cost is very expensive including cost of survey with an airplane. A large quantity of data obtained by CASI requires heavy processing.

Table 1. Representative satellite multispectral sensors, their spatial resolutions, swath width, band spectral ranges in nm of sensors and panchromatic bands, average revisit days and dynamic ranges.

Satellite	Spatial resolution (m)	Swath width (km)	Multi and panchromatic bands (nm)		Average revisit and dynamic range
WorldView-2 WorldView-3	WV-2 Pan 0.46 Multi 1.85 WV-3 Pan 0.34 Multi 1.38	WV-2 16 WV-3 13	Coastal Blue Green Yellow Red Red Edge NIR1 NIR2 Pan	400 – 450 450 – 510 510 – 580 585 – 625 630 – 690 705 – 745 770 – 895 860 – 1040 450-800	WV-2 3.7 days 11 bit/pixel WV-3 4.5 days 11 bit/pixel
GeoEye-1	Pan 0.41 Multi 1.64	15.2	Blue Green Red NIR Pan	450-510 520-580 655-690 780-920 450-900	3 days 11 bit/pixel
Quick Bird-2	Pan 0.61 Multi 2.4	16.5	Blue Green Red NIR Pan	450-520 520-600 630-690 760-900 450–900	3.5 days 11 bit/pixel
IKONOS	Pan 1 Multi 4	11.3	Blue Green Red NIR Pan	450-530 520-610 640-720 760-860 450-900	3 days 11 bit/pixel
Pleiades-1 Pleiades-2	Pan 0.5 Multi 2.8	20	Blue Green Red NIR Pan	450-530 510-590 620-700 775-915 480-820	4 days 12 bit/pixel
Spot-6	Pan 1.5 Multi 8	60	Blue Green Red	455-525 530-590 625-695	26 days 12 bit/pixel

Spot-7			NIR Pan	760-890 455-745	
LANDSAT 8 OLI	Pan 15 Multi 30	180	New Deep Blue Blue Green Red NIR Pan	433-453 450-515 525 – 600 630 – 680 845 – 885 500 – 860	16 days 12 bit/pixel
LANDSAT 7 ETM+	Pan 15 Multi 30	180	Blue Green Red NIR Pan	450-520 530 – 610 630 – 690 780-900 520 - 900	16 days 8bit/pixel
ALOS AVNIR-2 (Multi) PRISM (Pan)	Pan 2.5 Multi 10	70	Blue Green Red NIR Pan	420-500 520-600 610-690 760-890 520-770	46 days 8 bit/pixel

3.2. Availability of satellite images and software

Non-commercial satellite images of LANDSAT TM have been archived since 1972. Downloading digital data of LANDSAT 1-5 MSS, LANDSAT 4-5 TM, LANDSAT 7 ETM+ and LANDSAT 8 OLI is via internet by University of Maryland (http://glcfapp.glcf.umd.edu:8080/esdi/index.jsp) or United States Geological Survey (http://earthexplorer.usgs.gov) for free of charge. Due to problem of sensor, the present LANDSAT 7 ETM+ hasn't supplied any good images for remote sensing since 2002. In 2006, non-commercial satellite, Advance Land Observation Satellite (ALOS), launched by JAXA has a multispectral sensor, AVNIR-2, with 10 m spatial resolution and a panchromatic sensor, PRISM, with 2.5 m spatial resolution. These sensors that have spatially more precise than those of LANDSAT 7 ETM+ permit us to map coastal areas with various ecosystems and fishing activities. While ALOS has been out of service since April 2011 because of electric power depletion, archives of ALOS AVNIR-2 from 2006 to 2011 are available. NASA launched LANDSAT 8 that is successor of LANDSAT 7 in 2013. LANDSAT 8 OLI (Operational Land Imager) has higher radiometric and spectral resolutions and more visible bands, which allow us to map coastal habitats by analyzing their images.

Commercial or slightly costing satellite images are also available. World View 2/3, Geo Eye-1, Quick Bird-2, IKONOS and Pleiades-1/2 have multiband images with very high resolution (Table 1). There is a lot of commercial software for remote sensing such as ENVI, ERDAS Imagine, TNTmips, etc. Although their academic prices are reasonable, they are still expensive. Free software for remote sensing and GIS is also available via internet such as GRASS (http://grass.fbk.eu/index.php) and Multispec (https://engineering.purdue.edu/~biehl/MultiSpec/). They are software as effective as commercial software.

4. Ground- truthing of sea bottom

Ground truth is to obtain a coverage data of location *in situ* and in reality corresponding to a pixel on satellite image in order to verify contents of the pixel on the image on land. While, in the sea, we use sea truth instead of ground truth on land, it is better to use ground truth for verifying bottom surface covers on the bottom ground. When we classify the image, it is needed to know classification is successful or not. In this case, we use sea truth data for determining an accuracy of the classification to minimize errors in the classification.

Ground-truthing is conducted on site, performing bottom observations and measurements of substrates covering resolution cells studied on the remotely sensed digital image. The observations require highly accurate GPS to plot substrates on the geographic coordinates. For geometric correction of image, we also measure some typical locations that we can identify on the satellite image with a highly accurate GPS. These locations are called as Ground Control Points (GCPs) used for geometric correction. Software for remote sensing provides a function for the geometric correction with position data of GCPs as mentioned later.

Ground truth data are indispensable for supervised classification of an image. When data of bottom cover types with location are available, they can allocate attributes of pixels corresponding to their locations on an image. The spectral characteristics of pixels of the image corresponding to bottom covers on these sites are used for decision rules for classifying the other pixels of the image. In most cases, we divide ground truth data into two groups: one for training and the other for classification success. The latter data is to make an error matrix to evaluate the accuracy of the classification.

Mapping methods of seagrass beds are classified into two categories. One is a direct observation or measurement by researchers. The other is an indirect method using a remote sensing apparatus. Direct methods are ground-truthing surveys (walking, diving, grabbing, camera or video). In France, observation from a submarine was used to map lower bottom depth limit of *P. oceanica* beds along the French Riviera Coast (Meinesz and Laurent, 1978) because *P. oceanica* beds extend to bottom depths of 30-40 m. Direct methods are not efficient because they need time and persons to perform field surveys. Indirect methods are classified into acoustic and optic ones (Komatsu *et al*., 2003b). The former method includes echosounder, sidescan sonar and multibeam sonar. Echosounder can obtain echograms that are vertical acoustic profiles showing vertical distribution of seagrass beds. Komatsu and Tatsukawa (2006) used echosounder to map Zostera marina beds in Ajino Bay in Seto Inland Sea. Sidescan sonar can obtain horizontal images of bottom surface like aerial photography using ultrasounds. Sagawa *et al*. (2008) used sidescan sonar to map horizontal distributions of seagrass beds in Funakoshi Bay, Sanriku coast, Japan. They could classify two species of seagrasses based on acoustic shadow lengths of short *Zostera asiatica* Miki and long *Z. caulescens* Miki. Narrow multibeam sonar can map bottom topography using several decadal or hundred narrow sound beams. Komatsu *et al*. (2003) mapped seagrass beds in Otsuchi Bay, Sanriku coast, Japan.

Before presenting both methods, it is necessary to explain localizing positions where direct or indirect

methods are applied.

4. 1. Localization of ground-truthing sites in situ

It is very important to localize geographical positions of ground-truthing sites as precise as possible because we use these positions for classifications and/or evaluation of classification of bottom substrates. The Global Positioning System (GPS) became available in 1980s. It permits us to localize instantaneously a geographical position of a ground-truthing site. The accuracy of GPS has been ameliorated from 36 m (95% confidence level) to 6 m (95% confidence level) since 2000 because of the removal of Selective Availability (SA) from GPS (stopping the intentional degradation of the GPS signals) on 2 May 2000. In the world, 34 countries have already installed Differential GPS (D-GPS) radio beacon networks in territory of each country, and more are considering the adoption of this navigation standard. The improvement of the basic GPS signal through elimination of SA may allow the D-GPS radio beacons to transmit fewer error corrections and more accurate localization. Accuracy of D-GPS is about several decadal centimeters.

Another system to ameliorate precision of localizations with GPS is a satellite-based augmentation system (SBAS), such as European Geostationary Navigation Overlay Service (EGNOS), complement existing global navigation satellite systems (GNSS) (Table 2). The SBAS concept is based on GNSS measurements by accurately-located reference stations deployed across an entire continent (Figure 6). The GNSS errors are then transferred to a computing center, which calculate differential corrections and integrity messages which are then broadcasted over the continent using geostationary satellites as an augmentation or overlay of the original GNSS message. Several countries or a region have implemented their own satellite-based augmentation system. The SBAS can augment precision of positions within 1 m to 0.5 m.

Table 2. Satellite-based augmentation systems (SBASs) provided by a region or countries

Country or region	Name of satellite system
Europe	European Geostationary Navigation Overlay Service (EGNOS)
USA	Wide Area Augmentation System (WAAS)
Japan	Multi-functional Satellite Augmentation System (MSAS)
India	GPS and GEO Augmented Navigation (GAGAN)
Russia	System for Differential Corrections and Monitoring (SDCM)

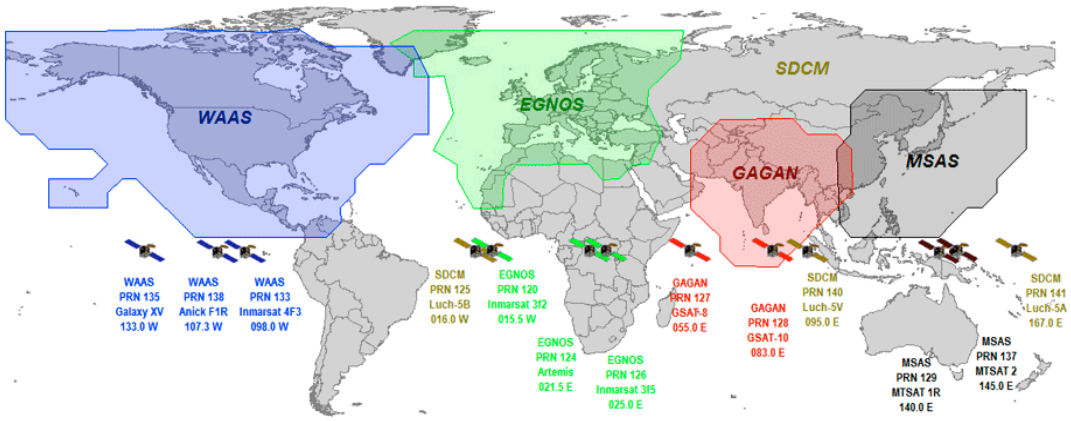

Figure 6. Area covered by different SBAS systems in the world (Source: http://sxbluegps.com/technology/sbas-made-easy/)

On 11 September 2010, the Japan Aerospace Exploration Agency (JAXA) launched the Quasi-Zenith Satellite System (QZSS) called “Michibiki”. It is a proposed three-satellite regional time transfer system and Satellite Based Augmentation System for the Global Positioning System, which would be receivable within Japan. Now only one Michibiki flies along an orbit of eight shape between Japan and Australia. JAXA will launch other three Michibiki satellites for covering Japanese area during 24 hours in the near future. At this moment, we can use Michibiki when it passes on Japan. It is estimated that the errors of localization are within 1 m. Some recent GPS can detect signals from Michibiki. It is recommended to use the GPSs which can receive Michibiki, SBAS and/or D-GPS with GLObal'naya NAvigatsionnaya Sputnikovaya Sistema (GLONASS) in Russia and BeiDou Navigation Satellite System in China because they are sold at reasonable prices.

4. 2 Direct methods

4. 2. 1. Walking and diving

When bottom depths are less than 1 m or tidal flats emerged from the sea surface, we can walk on the bottom to observe bottom substrates with GPS. It is very easy to obtain ground-truth data. On the other hand, it is needed to dive to observe the bottom when the sea level becomes high. Diving belongs to direct methods and is very sure for detecting bottom substrates. A merit of diving is to identify bottom covers, especially species compositions and densities of seagrass cover. However, it is laborious and not efficient to take data at many points. It is noted that the area observed by a diver is within several meters. When

another person measures positions of a diver from the boat with GPS, the error of positions becomes greater. This method can‘t be applied to turbid water areas.

4. 2. 2 .Manta tow

Manta tow is a simple method that a diver tracked by a boat takes continuous pictures as shown in Figure 7. When we use a boat, this method is very useful to take ground-truthing data at places where water clarity is high. A diver takes pictures with a digital camera from the sea surface at intervals of several seconds. If the time of camera is synchronized with a GPS, we can map bottom pictures on a geographical chart. GPS put in a plastic bag is fixed on the head of diver not to submerge it under the sea for receiving GPS signals.

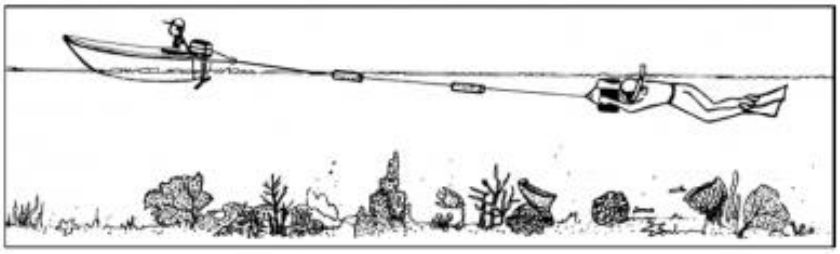

Figure 7. A schematic view of manta tow (Source: http://yunita-arum.blogspot.jp/2012/01/ekosistem-terumbu-karang-di-indonesia.html)

4. 2. 3. Video observation

Video observation is sometimes called as a drop camera observation. It is easier than diving observation. We lower the camera and monitor bottom features. It is better that the person who lowers the camera has GPS on his pocket to identify positions of camera. Time of camera and GPS must be synchronized. This observation is sensitive to turbidity.

Figure 8. Pictures showing video camera system for sea-truthing in Akkeshi Bay, east Hokkaido. Underwater video camera is lowered from the boat (left picture). An observer monitors bottom features by the display in the cabin (right picture)

4. 2. 4. Video towing

Recently, towing video camera system has been developed (Norris *et al*., 1997). The camera is mounted in a 'down-looking' orientation on a towfish, which was deployed directly off the stern of the vessel using the cargo boom. However, it is also sensitive to turbidity.

4. 3. Indirect methods

4. 3. 1. Echosounder

Echosounders have been developed to detect distributions of fish schools and to measure underwater bottom topographies. They send out ultrasonic waves of a certain frequency in the water and measure their reflection from bottoms and objects in the sea. Because the reflection coefficient of ultrasonic depends on materials of objects, especially air content in leaves of seagrasses, we can identify the objects in clear cases.

The echosounders have advantages not only to continuously measure biomass distributions and bottom topographies, but also to be used at a low cost and easy treatment. This method has been applied to several studies in phanerogam beds in lakes (Duarte, 1987), *Zostera marina* L. beds (Hatakeyama and Maniwa, 1978; Komatsu and Tatsukawa, 1998) (Figure 9) and *P. oceanica* meadows (Colantoni *et al*., 1982; Rey and Diaz del Rio, 1989).

Colantoni *et al*. (1982) tried to use a low frequency echosounder (3.5 kHz); it proved to be rather ineffective to discriminate the acoustic character between *P. oceanica* bed and the bottom. Although the high-resolution continuous seismic reflection (3.5 kHz) could distinguish the *P. oceanica* and others (Rey and Diaz del Rio, 1989), long wavelength of ultrasonic brings worse vertical precision of echosounder. Echosounders with an ultrasonic wave of 200 kHz is more appropriate for detecting seagrass beds (Figure 9) (Hatakeyama and Maniwa, 1978; Komatsu and Tatsukawa, 1998).

The echosounder can scan seagrass beds when traveling at about 1.0-1.5 m s^{-1} (2-3 knots). It is possible to investigate 37 km per day when a ship with an echosounder travels at 1 m s^{-1} (2 knots) for ten hours (Komatsu and Tatsukawa, 1998). In this way, the echosounder is a very useful apparatus to map seagrass beds.

Hatakeyama and Maniwa (1978) used the echosounder for mapping a *Zostera* bed, but they calculated only an index of biomass: sum of canopy heights by unit sector along transects scanned by the echosounder. Since it is necessary to estimate seagrass or seaweed biomass for a quantitative comprehension of the their ecosystems, Komatsu and Tatsukawa (1998) proposed a simple converting method from the shading grades of seagrass on echograms to above-ground biomass based on quadrat samplings (Figure 10). From these echograms, we can extract locations of seagrass and others for satellite remote sensing.

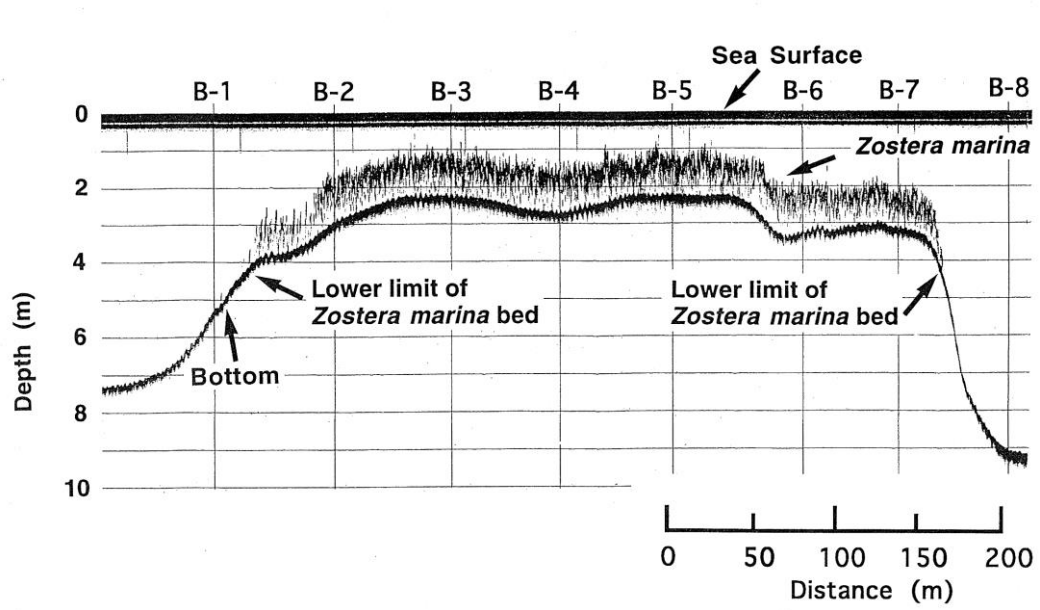

Figure 9. Raw records of echo trace along a transact in Ajino Bay, Japan cited from Komatsu and Tatsukawa (1998). A depth of 0 m is the sea surface, which is not standardized to the depth relative to the mean sea level.

The position of the lower bottom depth limit of seagrass beds is related to the light extinction coefficient influencing the minimum degree of light required for growth of seagrass (Duarte, 1991). Thus, it can be used for an indicator of water quality. In France, the lower bottom depth limit of *P. oceanica* was monitored by placing concrete markers (Meinesz, 1977). In this case, obtained results are very precise, but the observed area is limited. The echosounder can be used to define the vertical distribution of seagrass bed and the lower bottom depth limit of seagrass beds by correcting depths measured by the echosounder to the mean sea level. Therefore, monitoring of the lower bottom depth by the echosounder is useful for detecting the lower bottom depth limit of seagrass beds not precisely but roughly in a wide area. When these two types of monitoring are coupled, they complement each other to obtain lower bottom depth limits.

Komatsu and Tatsukawa (1998) clarified that the canopy height was nearly proportional to the maximum blade length (Figure 10). By cropping blades of seagrass, the height of seagrass canopies on the echo-traces can be used as an indicator of the maximum blade length of seagrass when the current speeds were not greatly different over the beds. Tanaka and Tanaka (1985) also reported a similar proportional relation between the canopy height and maximum frond lengths of *Sargassum* species.

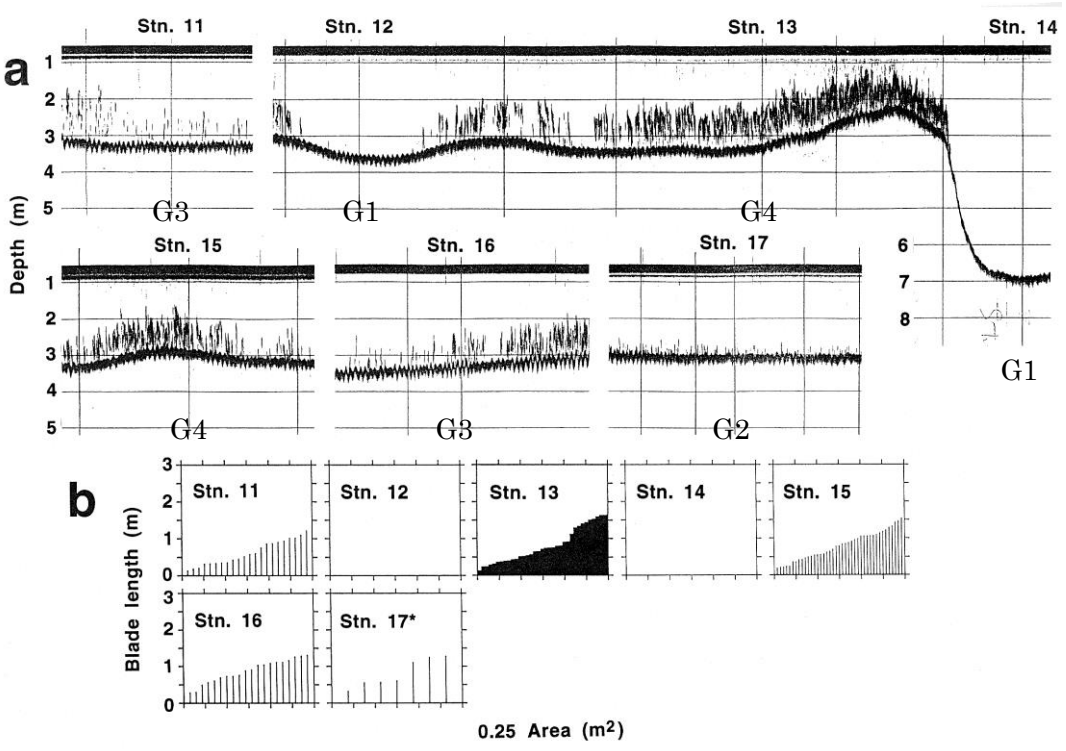

Figure 10. Echogram (upper panels) and blade length distribution (lower panels) obtained by a quadrat

sampling of 0.5 x 0.5 m at Stations 11-17 (Komatsu and Tatsukawa, 1998). The mark "*" indicates transformed data from quadrat sampling of 1x1 m to that of 0.5 x 0.5 m due to small quantity of seagrass shoots. Grades of echo traces of seagrass beds were shown at the lower part of the vertical line representing the station by the following characters: G1: Grade 1 (no seagrass); G2: Grade 2 (sparse seagrass); G3: Grade 3 (intermediate dense seagrass); G4: Grade 4 (dense seagrass). Blades lengths are shown as vertical lines from the smallest one to the largest one in order in each Figure at the stations (lower panels).

4. 3. 2. Sidescan Sonar

One acoustic method to map seagrass beds using a side scan sonar, which is more efficient than that of the ground surveys, has been developed since 1970s in the Mediterranean Sea. It scanned sea bottom at a width ranging 50-500 m, and could distinguish seagrass bed distributions and the others successfully (Newton and Stefanon, 1975; Meinesz *et al*., 1981; Lefèvre *et al*., 1984; Gloux, 1984; Ramos and Ramos-Espla, 1989; Pasqualini *et al*., 1998). Figure 11 and Figure 12 show a towing apparatus of side-scan sonar and the distribution map of *Z. caulescens* in Koajiro Bay in Sagami Bay obtained by the side-scan sonar, respectively. The patch structures are clearly depicted. However, it is difficult for this method to measure densities and heights of plants along a transect.

Sagawa *et al*. (2008) proposed use of sidescan sonar image as ground-truth data. They surveyed seagrass beds and examined accuracy of results obtained from satellite images from sidescan sonar image. They verified that maps surveyed with a sidescan sonar provides horizontal distributions of seagrass beds and proposed central areas (not border area) as ground truthing locations with and without seagrass beds.

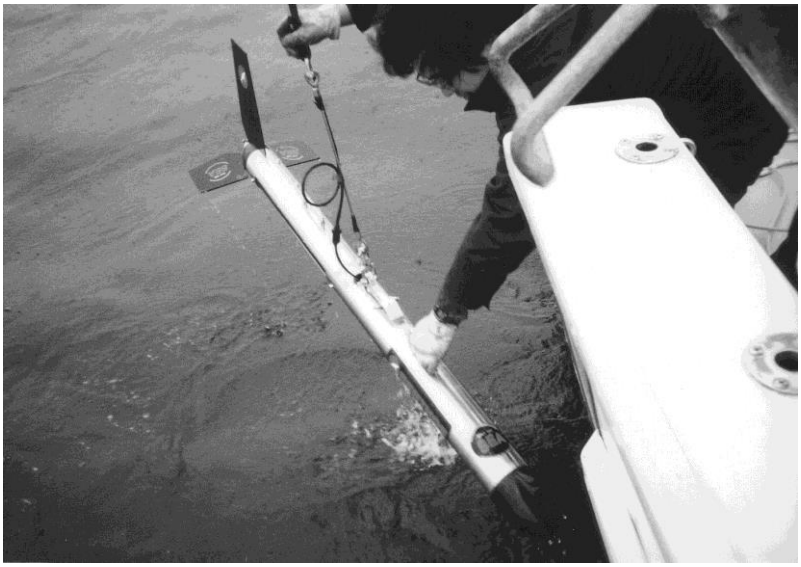

Figure 11. Picture showing towing transducer of side-scan sonar (Komatsu *et al*., 2003b)

Figure 12. Map showing horizontal distribution of *Zostera caulescens* surveyed by side-scan sonar (Komatsu *et al*., 2003b).

4.4. Seagrass cover and standing crop

Recently, satellite multiband images with high radiometric and/or spatial resolutions are obtained as reasonable prices. Using these data, researchers have studied to create maps of seagrass cover and/or seagrass standing crop. Estimation of seagrass covers or standing crop require ground truthing data. This section explains how to obtain ground-truthing data for this purpose.

In general, seagrass studies use a destructive sampling with a quadrat to examine species compositions, shoot densities, above- and below-ground biomasses, leaf lengths, leaf area index and so on. The main disadvantage of the destructive sampling is that it takes much time to take samples in situ and analyze samples in a laboratory. Remote sensing studies require many ground truthing data. Thus, non-destructive sampling using visual assessment techniques are applied to collect data for remote sensing studies.

Seagrass cover

Percentage cover of seagrass is estimated using a quadrat (e.g. McKenzie, 2003). This method is to

take digital pictures of seagrass on a quadrat of 0.5 x 0.5 m in situ and classify seagrass covers into percentage cover by using standardized pictures f seagrass covers. This method is quite repeatable when currents are weak and seagrass blades have a vertical orientation. However, the method becomes potentially unreliable when current strength increases and forces the seagrass canopy into a progressively horizontal (flattened) plane (Mumby *et al*., 1997a).

Seagrass standing crop

Mumby *et al*. (1997a) propose an alternative method to estimate seagrass standing crop based on Mellors (1991). An intensive 3-day training period was undertaken prior to survey work. After a broad reconnaissance survey, a provisional biomass scale was established following the methods of Mellors (1991). A quadrat of 0.5 x 0.5 m is placed in an area with the lowest discernible biomass and was given the category 1. The next quadrat is placed in seagrass which was both densest and possessed greatest blade length. This was assigned a category of 6. Quadrats for categories 2, 3, 4 and 5 are placed by estimating a linear interpolation between categories 1 and 6. Three divers conduct surveys using the technique by haphazardly throwing quadrats and comparing categories. Over 100 quadrats are cross-compared in this fashion until inter-observer agreement is highly consistent (complete agreement on approximately 95% of occasions). At this point, an adequate 1-6 scale is deemed to have been established and 4 quadrats of each category are excavated for calibration purposes. The quadrats are located haphazardly (i.e. pseudo-randomly) and encompassed a range of seagrass species composition rates if they are more than one species. Harvested seagrass is washed in fresh water and sorted to remove detritus and sediment. Each sample is divided by species and then sub-sampled for biomass categories 4-6 if it takes time to examine all seagrass in a quadrat of these categories. Sub-sampling is not necessary for most of the samples from categories 1-3. Epiphytes are removed from seagrass blades using either 5% citric acid or vinegar. Samples are oven-dried at 80°C for 48 h and weighed to the nearest 0.1 g using an electronic balance. Epiphyte-free total dry weights are calculated for each quadrat. It is important not to confuse percent cover or density with standing crop estimation. Although density and biomass arc closely related, the determination of standing crop also takes into account blade length and the relative dry weight of each species. From a practical perspective, the assessment is carried out by considering the entire 3-dimensional standing crop within the quadrat (i.e. a volume of seagrass above the sediment). In their case, the highest standing crop categories of 5 and 6 differ mainly in blade length rather than density. They recommend making a photographic record of the calibration quadrats which can be laminated and taken underwater for guidance.
The seagrass standing crop is plotted with ordinal scale (categories 1-6) for calibration of the scale. Mumby *et al*. (1997a) obtained the regression line by transforming standing crop data with a modified square root function with a good coefficient of determination. Using this regression, visual assessment surveys on seagrass can bring standing crop data.

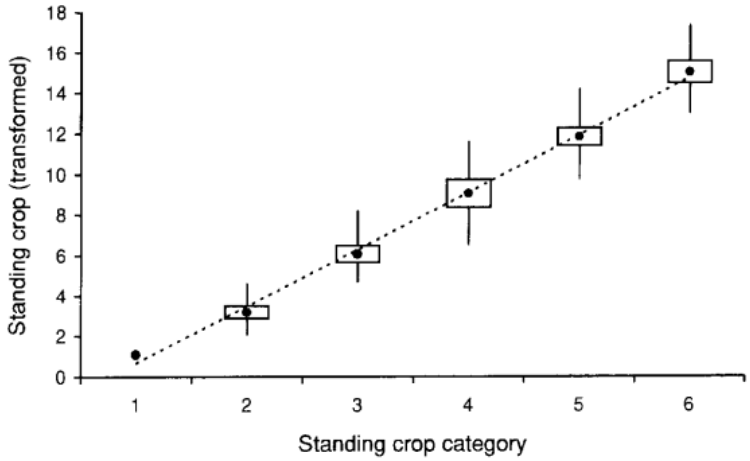

Figure 13. Calibration of ordinal scale for estimating seagrass standing crop (Mumby *et al*., 1997a). The mean 95% confidence intervals of the mean and range are shown from calibration data of each category. The variance within actual dry weights has been stabilized using a modified square-root transformation ($x'=\sqrt{(x+3/8)}$). Coefficient of determination, r^2=0.94 (n=103), actual standing crop (g m^{-2}). (Source: Mumby *et al*., 1997a)

5. Preparation for processing satellite images

5.1. Geometric correction

Satellite sensors project three dimensional surface of the earth to a plane. Satellite data were generally geocoded with WGS 84 coordinate system. Therefore, it is necessary to adjust a spherical surface to a horizontal plane. In most cases, remote sensing uses Universal Transversal Mercator (UTM) projection. In the plane of UTM, x axis and y axis represent east and north directions. UTM system has a zone number depending on longitude of an area by every six degrees from zone No. 1 between 180°W and 174°W to zone No. 60 between 174°E to 180°W. However, geometrical correction is needed to fit the image to the UTM coordinate system. This correction is based on more than six GCPs whose longitude and latitude have already been precisely obtained. In some cases, it is necessary to measure longitude and latitude of some discriminative points on the ground with D-GPS. If no GCPs are available, we select some alternative points on the map as GSPs. We relate GCPs with the corresponding points on the satellite image with software for remote sensing. This operation is called as geometric correction. It is recommended that GCPs are scattered and also placed at edges and corners of structural object or roads for analysis.

5.2. Digital number to radiance

The DN values recorded by a sensor are proportional to upwelling electromagnetic radiation. The majority of image processing has been based on raw digital number (DN) values in which actual spectral radiances are not of interest (*e.g.* when classifying a single satellite image). However, there are problems with this approach. The spectral signature of a habitat expressed as DN values is not transferable because the values are image specific under viewing geometry of the satellite when the image was pictured, the location of the sun, specific weather conditions, etc. We can't compare the values among the images taken at different time (*e.g.* seasons, years) by different satellite sensors (*e.g.* LANDSAT TM, AVNIR-2, IKONOS) and on the area of study larger than a single scene. Thus, it is necessary to convert the DN values to spectral units that are universal among different satellite images. If we obtain the spectral signature of substrate types, we can compare "spectral libraries" - *i.e.* libraries of spectral signatures containing lists of habitats and their reflectance. Converting the DN values to spectral units, we can refer calibration equations depending on satellite sensors that are included in the image data. In an example of IKONOS, the following conversion equation is generally used (Taylor 2005):

$$L_i = D_i \,/\, C_i \quad , \tag{1}$$

where L is the radiance at the sensor aperture (mW cm^{-2} sr^{-1}), C is the in-band radiance calibration

coefficient (cm^2 sr mW^{-1}) and *D* is the DN value. In the equation the subscript *i* represents spectral band *i*. Spectral radiances can be obtained from the calibration equation (1). USGS also provides the following equation for converting DN to radiance of LANDSAT 8 OLI (USGS, 2014).

$$L_i = M_{Li} D_i + A_{Li} \quad , \tag{2}$$

where M_{Li} and A_{Li} are band-specific multiplicative rescaling factor and band-specific additive rescaling factor of band *i* from the metadata, respectively. These radiances are those at the top of atmosphere (TOA). DN of LANDSAT 8 OLI can be also converted to TOA reflectance as the following equation (USGS, 2014):

$$\rho\lambda_i = \frac{M_{\rho i} D_i + A_{\rho i}}{\cos(\theta_{SZ})} = \frac{M_{\rho i} D_i + A_{\rho i}}{\sin(\theta_{SE})} \tag{3}$$

where $M_{\rho i}$ and $A_{\rho i}$ are band-specific multiplicative rescaling factor and band-specific additive rescaling factor of band *i* from the metadata, respectively. θ_{SZ} and θ_{SE} are local sun elevation angle of the scene center in degrees provided in the metadata and local solar zenith angle, respectively.

5. 3. Masking land areas and deep waters

It is necessary to exclude the land from satellite images for classification of coastal habitats to avoid miss-classification of seagrass beds. Near-infrared bands are easily absorbed by the sea surface while reflected by the land surface (Figure 14). Thus, we use DN, reflectance or radiance of an infrared band on the image to discriminate the sea from the land. If ponds or lakes are distributed on land, we need to manually mask them.

Deep waters are also excluded with red or green bands because they are absorbed with shallow water column. The deeper water areas indicate constantly lower values of their DN, reflectance and radiances. Thus, deep water areas can be classified with a certain threshold value. At the same time, it is needed to pay attention not to exclude seagrass and seaweed beds because seagrass and seaweed beds also show their lower values.

5.4. Atmospheric correction

The spectral radiances are those measured at the satellite sensor. Figure 4 shows that electromagnetic radiation observed by the satellite sensor has already passed through the Earth's atmosphere twice (sun to

target and target to sensor). During this passage, the radiation is affected by absorption which reduces its intensity and scattering which alters its direction. Absorption occurs when electromagnetic radiation interacts with gases such as water vapor, carbon dioxide and ozone. The electromagnetic radiation is scattered when it hits both gas molecules and airborne particulate matter (aerosols). Scattering will redirect incident electromagnetic radiation and deflect the reflected radiation from its path. Scattering also creates the adjacency effect in which the radiance recorded for a given pixel partly incorporates the scattered radiance from neighboring pixels. In order to make a meaningful measure of radiance at the Earth's surface, the atmospheric interferences must be removed from the data. This process is called atmospheric correction. There are some sophisticated models of atmospheric corrections such as 5s and 6s models (*e.g*. Tanre *et al*., 1990; Vermote *et al*., 1997), etc. After the atmospheric correction, light signals from the earth surface become clearer.

Spectral radiance will depend on the degree of illumination of the object (*i.e*. the irradiance). Then, the spectral radiance of features on the ground obtained by the atmospheric correction is usually converted to reflectance, which is called surface reflectance meaning the reflectance of the surface of the Earth. The reflectance is a ratio of radiance to irradiance on a certain surface. Be careful that surface reflectance is not that on the sea bottom.

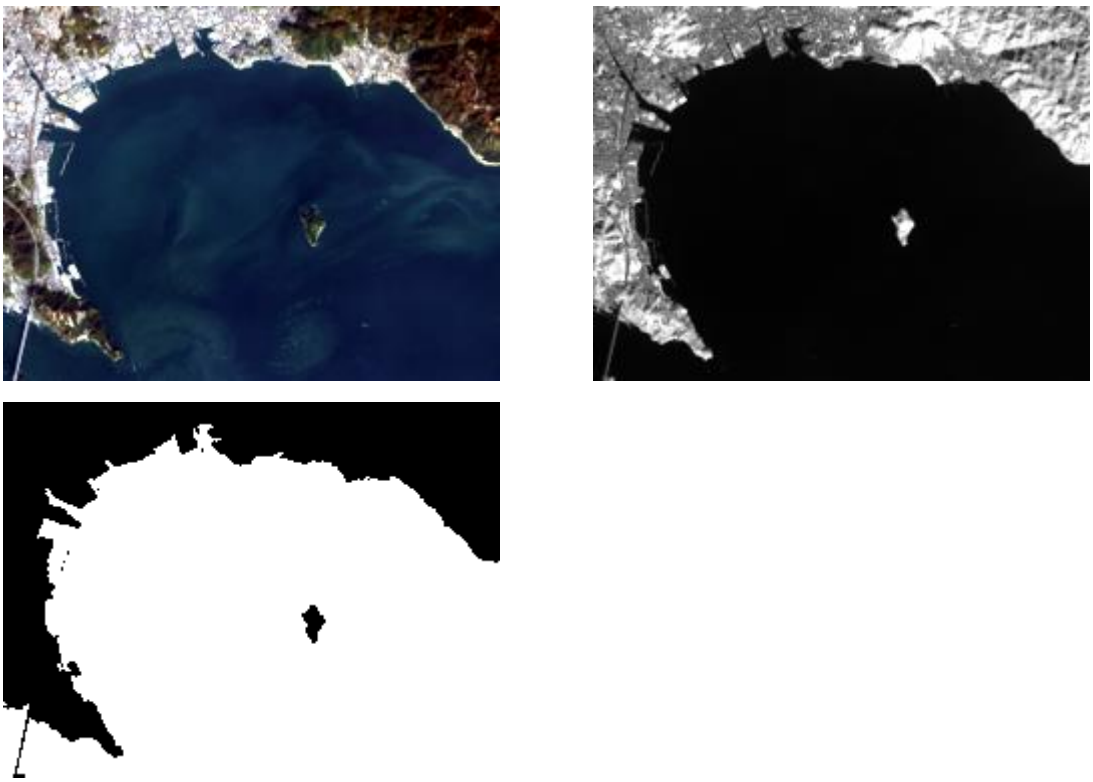

Figure 14. LANDSAT 8 OLI images of true color (upper left), band 5 (upper right) and mask (lower) on Ajino Bay, Japan. The mask was produced from pixels with DN values less than 7000.

5.5. Water column correction

In coastal waters, Lyzenga's model has been often used for water column correction because this model's simplicity and effectiveness. In the scope of radiometric correction, each pixel value within the image (DN value) is converted into a radiance value as mentioned above. From an optical perspective, bottom type can be identified by its reflectance. According to Lyzenga (1978), the relationship between the radiance level recorded by an optical sensor and bottom reflectance is expressed by the following equation:

$$L_i = L_{si} + a_i r_i \exp(-K_i gZ) \quad (4)$$

where L is the radiance same as in the equations (1) or (2), L_s is the radiance recorded over deep water (external reflection from the water surface and scattering in the atmosphere), a is a constant which includes the solar irradiance, the transmittance of the atmosphere and the water surface, and the reduction of the radiance due to refraction at the water surface (mW cm^{-2} sr^{-1}), r is the bottom surface reflectance, K is the effective attenuation coefficient of the water (m^{-1}), g is a geometric factor to account for the path length through the water and Z is the water depth (m). The value of g can be geometrically calculated from sun and satellite zenith angles at the moment when the satellite image was taken. Bottom differences are mirrored by variations in L, as r changes according to the bottom type. A radiometric correction index is required for estimating r. We introduce two types of simple radiometric correction suitable for coastal mapping: depth-invariant index proposed by Lyzenga (1981) and reflectance index proposed by Sagawa *et al*. (2010).

Depth-invariant index

In order to remove light scattering and absorption effects within both the atmosphere and the water body, Lyzenga (1981) suggested the calculation of a depth-invariant index. This index is expressed as follows:

$$Index_{ij} = \frac{K_j \ln(L_i - L_{si}) - K_i \ln(L_j - L_{sj})}{\sqrt{K_i^2 + K_j^2}} \quad (5)$$

where L, L_s and K are the same as in equation (4), this time with the i and j subscripts corresponding to two different bands of satellite image. Equation (5) is derived from equation (4) and refers simultaneously to two bands (bands i and j). For calculating this index, ratios of attenuation coefficients between bands are necessary. These coefficients were derived from ground truth data collected for a sandy bottom along a

bottom depth gradient (Lyzenga 1981). Using ground truth data, we can plot satellite data against bottom depths for sandy bottom type. The regression curve of Lyzenga's model is then obtained. When ground truth data are not available, we estimate sandy bottom and bottom depth from the sea chart if it exists. When the sea chart is not available, we estimate K_j/K_i as follows. Equation (5) can be transformed to equation (6) through dividing numerator and denominator with K_i:

$$Index_{ij} = \frac{K_j / K_i \ln(L_i - L_{si}) - \ln(L_j - L_{sj})}{\sqrt{1 + K_j^2 / K_i^2}} \quad , \tag{6}$$

where $\ln(L_i\text{-}L_{si})$ and $\ln(L_j\text{-}L_{sj})$ are dependent variables of bottom depths from equation (4). If we can obtain reflectances of band *i* and *j* at the same pixels on a satellite image, $\ln(L_i\text{-}L_{si})$ and $\ln(L_j\text{-}L_{sj})$ on pixels interpreted as the sand bottom are plotted them on horizontal axis and vertical axis, respectively. The regression line of points between $\ln(L_i\text{-}L_{si})$ and $\ln(L_j\text{-}L_{sj})$ gives K_j/K_i as its slope.

Bottom reflectance index

In order to improve mapping accuracy, Sagawa *et al*. (2010) proposed an alternative reflectance index (Bottom Reflectance Index: BR index) expressed by the following equation:

$$BR\ index_i = \frac{(L_i - L_{si})}{exp(-K_i g Z)} \quad , \tag{7}$$

where *L*, *Ls*, *K*, *g* and *Z* are the same as equation (4).

To calculate this BR index, it is needed to combine bottom depth data, *Z*, with attenuation coefficient, *K*. We use each band attenuation coefficient same as for the Depth-invariant index. Concerning bottom depth data, the bathymetry map or sea chart supplied by local government or hydrographical institutions is referred. It may be reasonable to take advantage of these data, as they are easily available and represent generally accurate input. Once the numerator in equation (7) was replaced by $a_i\ r_i\ \exp(-K_i g Z)$ (from equation (4)) and the equation rearranged, the index becomes the following equation including bottom reflectance:

$$BR\ Index_i = a_i r_i \tag{8}$$

where *a* and *r* are the same as in equation (4) and *i* corresponds to a satellite image band *i*. Clearly, this

index is linearly related to bottom reflectance. As a result, we named it ‘reflectance index’. This index enables us to compare not only the difference in reflectance ratios between bands but also the difference in absolute reflectance for each band of satellite image.

According to Lyzenga (1978), equation (4) should not be applied to very shallow areas, as the model ignores internal reflection effects occurring at the water surface. Thus it is better to apply both radiometric corrections exclusively to areas deeper than about 1-2 m. On the other hand, we need not underwater but atmospheric radiometric correction when there are seagrasses exposed to the sea surface.

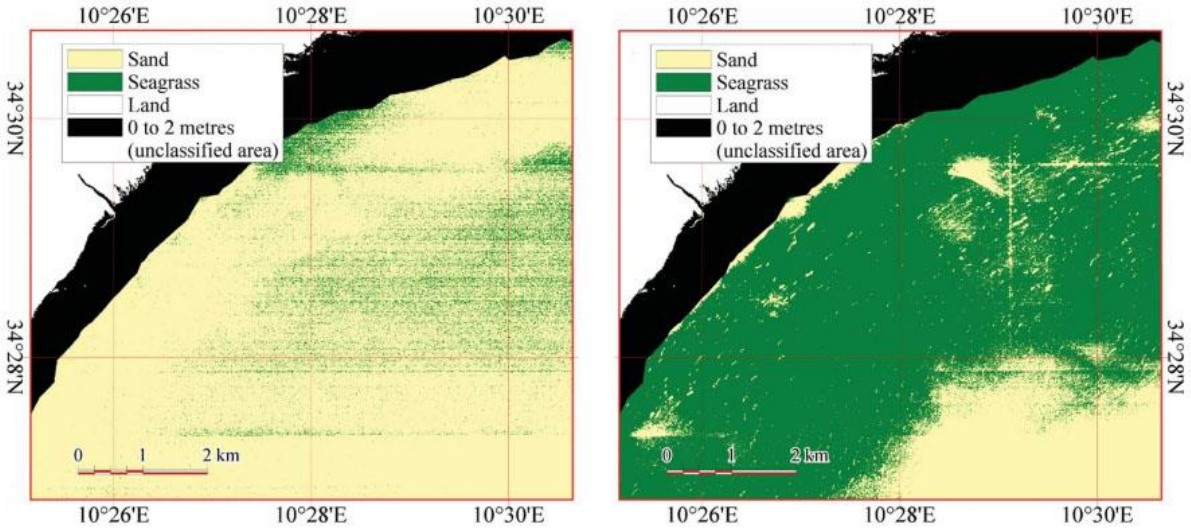

Figure 15. Maps derived from satellite image analysis (Mahares). Black areas, described as '0–2 meters (unclassified area)' in the legends, represent the data which were not included in our analysis. The maps are obtained by applying a radiometric correction based on (a) the traditional depth-invariant index; (b) the bottom reflectance index. (Source: Sagawa *et al*., 2010)

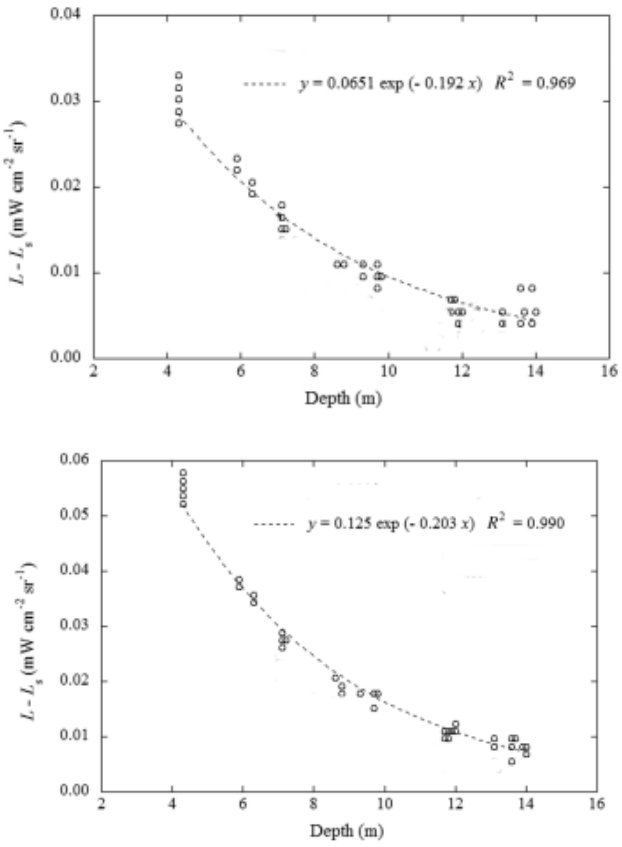

Figure 16. Relation between radiance level and depth blue (upper panel) and green (lower panel) on the sand bed (source: Sagawa *et al*., 2010)

Sagawa *et al*. (2010) applied both radiometric corrections of Depth-invariant index and Bottom Reflectance index to IKONOS image spotting seagrass beds off Mahares in Golf of Gabesz, south Tunisa, facing Mediterranean Sea, acquired on 2 October 2005. In this area, *Posidonia oceanica* L. is the most abundant and common species and it mainly occurs on a sandy bottom. Figure 15 shows results of supervised classification applied to Depth-invariant Index and Bottom Reflectance index to classify sand and seagrass. In these waters, water type was Jerlov Water Type II-III suggesting turbid waters (Figure 16). Overall accuracy of the former was 54% meaning random classification between two bottom types. On the other hand, that of the latter was over 90%. When the bottom depth distribution is available, radiometric correction using Bottom Reflectance index is very practical to map seagrass beds under turbid waters rather than Depth-invariant index. When water is clear, radiometric correction using Depth-invariant index can obtain good classification results. This is true because some studies showed good results applying Depth-invariant index for mapping of seagrass beds in Caribbean Sea (Mumby *et al*., 1998) or Mediterranean Sea (Pasqualini *et al*, 2005; Belluco *et al*, 2006; Fornes *et al*, 2006) where transparencies are very high.

6. Image classification

6.1 Pixel-based classification

In coastal habitat mapping, pixel-based classification consisting of supervised or unsupervised classification is generally applied to multiband satellite data after radiometric correction mentioned above. Most classifications for seagrass mapping have been created using a pixel-based analysis of satellite multiband images. They used either a supervised classification or unsupervised classification. These pixel-based procedures analyze the spectral properties of every pixel within the region of interest. Ground truth data concerning each bottom type distributions are required. These data must be prepared through ground-truthing such as diving, observation by a lowered camera from the ship, side scan sonar measurements, etc. as mentioned above and described by Komatsu *et al*. (2003b). If ground truth data are not available, unsupervised classification is useful. Unsupervised classification groups pixels into some categories with similar bottom reflectance though a statistical standard such as ISODATA etc. Using the unsupervised classification method, the software is instructed to create the number of clusters that is input before processing in the iterations that is input before processing the while attempting to meet a predetermined threshold value. By calculating and plotting the cluster statistics we can determine what number of clusters (or classes) to use. Usually, we determine the number of clusters more than classes that we need. After processing, some clusters are merged to one cluster when they represent a suitable class. Based on unsupervised classification, we can effectively conduct ground truth survey or field survey.

Mumby and Green (2000) stated that number of samples (ground truth data) necessary for one class with a supervised classification is 50 ground truth data corresponding to 50 pixels of image. Calculation of classification accuracy needs 30 ground truth data (30 pixels of image). Thus, a total of 80 ground truth data are needed for one class with a supervised classification. When we classify pixels into three classes, we need 240 ground truth data corresponding to 240 pixels of image. This is ideal case. Since we don't have enough time to take these samples, we use 25 to 30 samples for one class for supervised classification and 20 to 30 samples for one class for accuracy evaluation.

The classification of supervised classification is based on the spectral signature defined in the training set. The digital image classification software determines each class on what it resembles most in the training set. Supervised classification is based on the idea that a user can select sample pixels in an image that are representative of specific classes and then direct the image processing software to use these training pixels as references for the classification of all other pixels in the image. Training pixels are based on the ground truth data above-mentioned. The common supervised classification algorithms are maximum likelihood and minimum-distance classification. Maximum Likelihood method assumes that the statistics for each class in each band are normally distributed and calculates the probability that a given pixel belongs to a specific class. Each pixel is assigned to the class that has the highest probability (that is, the maximum likelihood). Minimum Distance method uses the mean vectors for each class and calculates the Euclidean

distance from each unknown pixel to the mean vector for each class. The pixels are classified to the nearest class.

6.2 Object-oriented classification

Recently, higher resolution satellite images such as WorldView2 and WorldView3 are available with reasonable prices as archived images. It is possible for classifications to take into account the spatial or contextual information related to pixels. Thus, the idea to classify objects stems from pixel-based classifications to object-oriented (or object-based) classifications based on groups of pixels with based on their internal homogeneity and spectral separability at multi-scale levels. The object-oriented analysis classifies objects instead of single pixels by multi-scale segmentation of pixels, which lead to the extraction of spectrally and internally homogeneous units at a particular scale. It includes image segmentation to identify image objects and classification of the identified image objects. Objects form a hierarchical and scale-dependent structure. This means that any object, in contrast to a pixel, has not only neighbors but also sub-objects and super-objects at different scales. Groups of pixels, due to their hierarchical structure, are able to include many attributes which can describe objects' intrinsic characteristics (using physical features like color, texture, and shape), typological characteristics (relations to other objects, sub-objects and super-objects) and context. Two representative softwares of object-oriented approach are ENVI EX (Exelis VIS) and eCognition (Trimble), which are based on edge to identify image objects and on FNEA (fractal net evolution approach) and multi-resolution segmentation, respectively (Xiaohe *et al*., 2014).

The object-oriented method was applied to seagrass mapping with images obtained from airborne digital cameras by Lathrop *et al*. (2006). Following Robbins and Bell's (1994) approach, they set habitat structure at three different levels: (a) meadow - a spatially continuous area of seagrass beds of varying percent of cover composition; (b) bed - a spatially continuous area of overall similar percent of cover composition; and (c) patch - a small discrete clump of seagrass- or gap - an area within a seagrass bed not occupied by plants.

Lathrop *et al*. (2006) developed a hierarchical classification scheme to multiband images in a shallow (mean depth of 1.5 m at mean lower-low water) back-bay lagoonal type of estuary on New Jersey's Atlantic coast taken by an airborn digital camera. Two GeoTiff image products were created, a true color imagery set and an infrared imagery set, both at a 1 meter ground cell resolution and 8-bit radiometric resolution. They broadened three different levels of seagrass to six levels including them: Level 1 of land and water, Level 2 of deepwater/channels (>1.5 to 2 m depth) and shallow water (<1.5 to 2 m depth) from water of Level 1, Level 3 of sand/mud flats (<1.5 to 2 m depth) and macrophyte from shallow water of Level 2, Level 4 of the macroalgae and seagrass meadows from macrophyte of Level 4, Level 5 of dense, moderate and sparse seagrass beds from seagrass meadows of Level 4, and Level 6 of seagrass patch and gap (bare bottom) of three seagrass levels of Level 5. Level 1 was classified with near-infrared band. Level 2 was classified a simple membership rule based on the bathymetry layer. Level 6 was obtained by segmenting

the whole area to fine scale objects using a scale parameter of 10. The image segmentation was then coarsened to merge areas of like classes using a scale parameter of 15 (for Level 5) and 30 (for Level 4). The Level 4 or 5 image objects were visually interpreted and manual encoded as to the appropriate bottom type based on the analyst judgment. If the field reference data was available, the analyst can consult them. Thus, level 4 to 6 are dependent of scales of image segmentation decided by scale parameters arbitrarily given. The size of the object is associated with its physical and biological spatial structure. A homogeneity criterion for smoothness and compactness of segmentation is based on a local variance of pixels to be grouped, given by a parameter. The seagrass density data for the 245 field reference points were categorized into four seagrass density classes (absent, sparse, moderate, and dense), compared with the same location from the classification result.

Urbański *et al*. (2009) analyzed Quickbird data for mapping seagrass beds in sandy shoal habitat in the southern Baltic Sea. The spatial resolution of the panchromatic band and multi-spectral bands are 0.6 m and 2.5 m, respectively. Their number and size at the particular segmentation level depend on a scale parameter. The segmentation process aims to retain objects of strong spectral and shape homogeneity. They segmented each panchromatic image for the following scale parameters: 400, 300, 200, 100, 50, and 20; which constitute six levels of objects as mentioned above. The homogeneity criterion was set to 0.9 for colour, 0.1 for shape, and 0.5 both for smoothness and compactness. They selected level of seagrass meadows, beds and patch/gap with scale parameters of 200, 20 and 10, respectively. They classified segments of seagrass bed level into five zones with a seagrass index (SGI) consisting of band 1, band 2 and standard deviation of band 2 of segment with a scale parameter of 20. Within each zone in the object layer with a scale parameter of 20 (patch/gap level), approximately 30 objects presenting vegetation cover (SAV) and approx. 30 objects without vegetation cover (notSAV) were selected by manual sampling. In order to perform accuracy assessments, samples from the patch/gap level were selected once more but for the scale parameter of 10. The samples were assigned to SAV or notSAV classes. They stated "Atypical, potentially difficult to classify objects were purposely chosen". A problem of object-oriented classification is to set parameters not objectively but subjectively and also needs manual choosing of segments. In many cases, seagrasses grow patchy and show their distributions as salt-and-pepper. In these cases, it is still better to apply a pixel-based classification with a high spatial resolution satellite images.

7. Validation of accuracy

One of the most important themes for seagrass mapping with a remote sensing is an accuracy evaluation of classification. In general, accuracies of classification are evaluated with an error matrix (confusion matrix or contingency table) (Mumby and Green, 2000). The accuracies are judged with a user accuracy, a producer accuracy, an overall accuracy and a tau coefficient (Ma and Redmond, 1995).

Error Matrix (Pixels and percent)

The error is calculated by comparing the class of each ground truth pixel with the corresponding class in the classification image. Each column of the error matrix represents a ground truth class and the values in the column correspond to the classification image's labeling of the ground truth pixels. Table 3 shows the class distribution in pixels and percentage for each ground truth class.

Table 3. Example of error matrix of seagrass mapping. Yellow cells represent diagonal components that are correctly classified. Numbers and those in parentheses are pixels and percentages of pixels, respectively.

	Ground truth data			
Satellite image classification data	Seagrass	Sand	Row total	User accuracy
Seagrass	14 (7)	6 (3)	20 (10)	14/20 (70)
Sand	86 (43)	94 (47)	180 (90)	94/180 (52.2)
Column total	100 (50)	100 (50)	200 (100)	
Producer accuracy	14/100 (14)	94/100 (94)		
Overall accuracy			108/200 (54)	
Tau coefficient			0.08	

User accuracy is a measure indicating the probability that a pixel is Class A given that the classifier has labeled the image pixel into Class A. User accuracies are shown in the rows of the error matrix. For example, in Table 3, seagrass class classified by the classifier has a total of 20 pixels where 14 pixels are classified correctly and 6 other pixels are classified incorrectly. The ratios of the number of pixels classified correctly (14) and incorrectly (6) into the seagrass class by the total number of pixels in the class of seagrass by the classfier (20) are 70% and 30% (Table 3), respectively, corresponding to a user accuracy and an error of commission.

The producer accuracy is a measure indicating the probability that the classifier has labeled an image pixel into Class A given that the ground truth is Class A. For example, in Table 3, seagrass class of ground truth has a total of 100 pixels where 14 pixels are classified correctly and 86 other pixels are classified incorrectly. The ratios of the number of pixels classified correctly (14) and incorrectly (86) into the seagrass

class by the total number of pixels in the ground truth class of seagrass (100) are 14% and 86% (Table 1), respectively, corresponding to a producer accuracy and an error of omission.

The overall accuracy is calculated by summing the number of pixels classified correctly and dividing by the total number of pixels. The pixels classified correctly are found along the diagonal of the error matrix table which lists the number of pixels that were classified into the correct ground truth class. The total number of pixels is the sum of all the pixels in all the ground truth classes. For example, in Table 1, pixel counts of diagonal components consist of 14 pixels of seagrass and 94 pixels of sand, meaning correctly classified pixels. The overall accuracy (54%) is obtained by dividing the correctly classified pixels number (14+94) by the total number of ground truth pixels (200).

Overall accuracy is the overall degree of agreement in the matrix. Generally, accuracies of classification of surface covers of coastal sea bottom are lower than those of land (*e.g*. Mumby et al, 1998). Mumby *et al*. (1999) stated that reasonable accuracy is between 60 and 80% for coarse descriptive resolution such as corals/seagrasses and mangroves/non-mangroves by using satellite images such as LANDSAT TM or pansharpened image of LANDSAT TM with SPOT. In any cases, overall accuracy is more than about 90% to monitor temporal changes in spatial distributions of bottom covers using a remote sensing (Mumby and Green, 2000).

Tau Coefficient

It is a reasonable way to describe the overall accuracy of a map but does not account for the component of accuracy resulting from chance alone. A chance component of accuracy exists because even a random assignment of pixels to habitat classes would include some correct assignments.

The Tau coefficient, T(e), is another measure of the accuracy of the classification to exclude a chance component and is expressed as the following equation:

$$T(e) = \frac{Pr(a) - Pr(e)}{1 - Pr(e)} \quad , \qquad (9)$$

where Pr(a) and Pr(e) are the relative observed agreement among classes and hypothetical probability of chance agreement. For example, in Table 3, Pr(a) corresponds to the overall accuracy, 0.54. Pr(e) derived from two classes is 0.5. Then, we can obtain T(e) as 0.08 by dividing (0.54-0.50) with (1.0-0.5). The Tau coefficient ranges between -1.0 and 1.0. When the Tau coefficient is -1.0 and 1.0, classification is of perfect discrepancy and agreement, respectively. When the Tau is between 0.41 and 0.60, classification is of moderate agreement. When the Tau is between 0.61 and 0.80, classification is of good agreement. When the tau is over 0.80, classification is of nearly prefect agreement.

The variance of Tau, σ^2, is calculated as the following equation (Ma and Redmond, 1995):

$$\sigma^2 = \frac{\mathrm{Pr(a)(1-Pr(a))}}{\mathrm{n(1-Pr(e))}^2} \quad , \qquad (10)$$

Confidence intervals are then calculated for each Tau coefficient at the 95% confidence level (1-α), using the following form:

$$95\%CI = T(e) \pm Z_{\alpha/2}\,(\sigma^2)^{0.5} \quad , \qquad (11)$$

where *Z* is a standard normal distribution with the lower bound of α/2. Using Table 3, we obtain 95%CI as 0.08 ±0.005. The coefficient's distribution approximates to normality and Z-tests can be performed to examine differences between matrices (Ma and Redmond 1995). Z-tests between Tau coefficients 1 and 2 (T_1 and T_2) are conducted using the following equations:

$$Z = \frac{T_1 - T_2}{\sqrt{\sigma_1^2 - \sigma_2^2}} \quad , \qquad (12)$$

where σ^2 is the variance of the Tau coefficient, calculated from equation (10). We can examine whether Tau coefficients have a 95% probability of being different or not.

8. Coverage and biomass estimation of seagrass

Some recent studies have documented methods for mapping seagrass species, cover and biomass properties from satellite images and field data (*e.g*. Baumstark *et al*., 2013; Urbański *et al*., 2010). Phinn *et al*. (2008) compared accuracies of seagrass percentage cover classification (1–10%, 10–40%, 40–70% and 70–100%) in the shallow sub-tidal areas of the Eastern Banks, Moreton Bay, Australia, among images of compact airborne spectrographic imager with a pixel size of 4 m x 4 m, a radiometric resolution of 14 bit and 16 bands (CASI), Quick Bird-2 with a pixel size of 2.4 m x 2.4 m, a radiometric resolution of 11 bit and 4 bands, and LANDSAT 5 TM with a pixel size of 30 m x 30 m, a radiometric resolution of 8 bit and 4 bands. The airborne hyper-spectral image data returned high accuracies across all cover levels from very high (70–100%) to very sparse (0–10%). In contrast, both Quick Bird-2 and LANDSAT 5 TM were unable to differentiate moderate to low (10–40%) and sparse (0–10%) levels of seagrass cover. In the LANDSAT 5 TM image data this was expected as a function of its relatively large pixel size, limited radiometric resolution and broad spectral bands. Phinn *et al*. stated that the band placement and slightly lower radiometric resolution of Quick Bird-2 than the CASI data, and reduced its ability to detect the small reflectance differences between seagrass cover.

Most of researches on seagrass biomass use relation between signals of multi bands from bottom substrates and seagrass covers or standing crops of seagrass. Seagrass covers and standing crops of seagrass are obtained by quadrat sampling of seagrass through field surveys. Mumby *et al*. (1997) used the DII as signals. If more than one DII are available, they applied principal component analyses to combine multiple DIIs into a single regressor (the first principal component). They obtained ground-truthing data by simple, precise, non-destructive and quick method for measuring seagrass standing explained in Section 4.4.

Above-ground biomass of seagrass has been estimated by remote sensing. Most of studies have converted pixel values of reflectance to above-ground biomass based on a regression between reflectance and biomass which have been obtained by quadrat sampling *in situ*. Mumby (1997b) compared performances of above-ground biomass estimation with use of regressions between field measurements of standing crop and Depth-invariant indexes of LANDSAT TM, SPOT XS and CASI images on seagrasses in the tropical Western Atlantic. They found that predictions were high coefficients of determination: 0.74, 0.79 and 0.81, respectively. Hashim *et al*. (2014) used LANDSAT 8 OLI image to map seagrass biomass in Johor Straight. After they classified seagrass beds, they mapped above-ground biomass of classified seagrass area based on a regression between BR Index and above-ground biomass of quadrat sampling of 0.5 x 0.5 m. They obtained good regression between them with a coefficient of determination of 0.93 (r^2) (see Figure 13).

For estimating above-ground biomass of seagrasses, it is necessary to consider their seasonal changes. When we compare biomass distributions among different locations and periods, we need to take luxurious and scanty growth seasons of seagrasses, interannual changes of timing of their growth and interannual changes in their distributions into account. Another problem is whether quadrat sampling of seagrass

biomass in only 0.5 x 0.5 m area represents biomass in a pixel or not. For example, one pixel of LANDSAT TM is 30 x 30 m. This pixel size includes not only quadrat sampling position but also other bottom covers, which produce a mixel effect. If seagrass beds are not homogeneous, quadrat samples are not representative of the pixel because of its broader area. If we use Quick Bird-2 or CASI, we encounter georeferencing problems of quadrat samples and pixels. When quadrat sampling is conducted *in situ*, its position is obtained with GPS. The position data by GPS include an error. Satellite and CASI images also include error in pixel positions. It is possible that a position of quadrat sampling is not identical to a pixel on satellite or CASI images. To solve this georeferencing problem, it is needed to use more accurate GPS system. When we estimate seagrass biomass roughly with satellite image analysis with quadrat sampling, an objective of biomass estimation must be clear.

9. Summary

Most of remote sensing studies on seagrass beds aim to map not only spatial distributions at a certain time but also temporal changes in spatial distributions from time to time. To conduct a reliable assessment of changes in seagrass extent and cover over time, the data sets compared should be based on specific requirements as shown in Table 4 (Roelfsema *et al*., 2013). In regards to assessing natural variability, intra vs. inter annual variation and algal presence, it is important that field sampling data and location, and date of remotely sensed data sets are considered.

We introduced simple methods to map seagrass beds. We would like to stress again that radiometric correction is very important for satellite remote sensing to map correctly bottom types. In tropical waters, water transparency is usually very high. Simple Lyzenga's Depth-invariant index is very useful. On the other hand, in temperate waters with low transparency, Bottom Reflectance index proposed by Sagawa *et al*. (2010) is better than Depth-invariant index.

At this moment, LANDSAT 8 OLI with 30 m spatial resolution is the only available and non-commercial satellite images provided by NASA, and can be applied to coastal habitat mapping without payment. Japan Aerospace Exploration Agency will prepare ALOS-3 that has higher spatial resolution than LANDSAT OLI. If this satellite is launched, seagrass mapping in the Northwest Pacific will be advanced enormously.

Table 4. Ideal requirements to conduct a reliable assessment of changes in seagrass extent and horizontal projected percentage seagrass cover over time. *The error that could occur when requirement is not adhered to. (Source: Roelfsema *et al*., 2013)

Ideal data set requirements	Error type*	Example of impact of error (DS1 = data set 1, DS2 = Data set 2)
Georeferenced	Position shift	Changes detected (false positives)
Near identical spatial extent	Missing data	If an area is not mapped for DS1 compared to DS2 due to missing data, it could be detected as a change
Identical mapping categories	Incomparable mapping categories	Qualitative versus quantitative categories
Identical mapping scale	Variation in level of detail	Small patches of seagrass are mapped in one and not in the other
Reproducible mapping method	Methodological error	DS1 based on manual digitisation, DS2 based on pixel based image classification
Seasonal sampling	Natural variation	DS1 in winter versus DS2 in summer
Similar tidal stage and water clarity	Affects ability to detect seagrass	Satellite image for DS1 was derived at high tide with turbid water, and for DS2 with low tide and clear water. Seagrass could be mapped in deeper water for DS2.
Replicate field sampling	Variation in calibration or validation	DS1 field data based on limited point based sampling, DS2 based on detailed transect sampling for same area.
Sampling accuracy	Decreased map quality	DS1 has high accuracy, versus DS2 with low accuracy resulting in low reliability

Acknowledgements

The author appreciates reviewers for their constructive comments. He also thanks to Dr. Tatsuyuki Sagawa of Remote Sensing Technology Center of Japan and Dr. Genki Terauchi of Northwest Pacific Region Environmental Cooperation Center for their critical reading of the manuscript.

References

Baumstark, R., Dixon, B., Carlson, P., Palandro, D. and Kolasa, K. (2013): Alternative spatially enhanced integrative techniques for mapping seagrass in Florida's marine ecosystem. International Journal of Remote Sensing, 34, 1248–1264.

Belluco, E., Camuffo, M., Ferrari, S., Modenese, L., Silvestri, S., Marani, A. and Marani, M. (2006): Mapping salt-marsh vegetation by multispectral and hyperspectral remote sensing, Remote Sensing of Environment, 105, 54–67.

Boudouresque, C.-F., Charbonel, E., Meinesz, A., Pergent, G., Pergent-Martini, C., Cadiou, G., Bertrandy, M.C., Foret, P., Ragazzi, M. and Rico-Raimondino, V. (2000): A monitoring network based on the seagrass Posidonia oceanica in the northwestern Mediterranean Sea. Biologia Marina Mediterranea, 7, 328-331.

Calvo, S., Frada Osterano, C. and Abbadessa, P. (1993): The suitability of a topographical instrument for an integrated approach to the cartography of Posidonia oceanica meadows. Oceanologica Acta, 16, 273-278.

Colantoni, P., Gallignani, P., Fresi, E. and Cinelli, F. (1982): Patterns of *Posidonia oceanica* (L.) Delile beds around the Island of Ischia (Gulf of Naples) and in adjacent waters. P.S.Z.N.: Marine Ecology, 3, 53-74.

Coles, R.G., Lee Long, W.J., Watson, R.A. and Derbyshire, K.J. (1993): Distribution of seagrasses, and their fish and penaeid prawn communities, in Cairns Harbour, a tropical estuary, northern Queensland, Australia. Australian Journal of Marine and Freshwater Research, 44, 193-210.

Costanza, R., d'Arge, R., deGroot, R., Farber, S., Grasso, M., Hannon, B., Limburg, K., Naeem, S., O'Neill, R.V., Paruelo, J., Raskin, R.G., Sutton, P., van den Belt, M. (1997): The value of the world's ecosystem services and natural capital. Nature, 387, 253–260.

Dennison, W.C., Orth, R.J., Moore, K.A., Stevenson, J.C., Carter, V., Kollar, S, Bergstrom, P.W. and Batiuk, R.A. (1993): Assessing water quality with submerged aquatic vegetation: Habitat requirements as barometers of Chesapeake Bay health. BioScience, 43, 86-94.

Duarte, C. M. (1987): Use of echosounder tracings to estimate the above ground biomass of submerged plant in lakes. Canadian Journal of Fisheries and Aquatic Sciences, 44, 732-735.

Duarte, C.M. (1991): Seagrass depth limits. Aquatic Botany, 40, 363-377.

Duarte, C. M. and Kirkman, H. (2001): Methods for the measurement of seagrass abundance and depth distribution. In Global seagrass research methods, edited by Short, F. T., Short, C. A. and Coles, R. G. pp. 141-153, Elsevier B.V., Amsterdam.

Dierberg, F. E. and Kiattisimkul, W. (1996): Issues, impacts, and implications of shrimp aquaculture in Thailand. Environmental Management, 20, 649-666.

Fredj, G., Meinardi, M., Pierrot, S. and Roy, P. (1990): Cartographie par le satellite SPOT 1 de communautés benthiques littorales en Méditerranée occidentale. Bulletin de l'Institut

océanographique de Monaco, 6, 71-85.

Fornes, A., Basterretxea, G., Orfila, A., Jordi, A., Alvarez, A. and Tintore, J. (2006): Mapping Posidonia oceanica from IKONOS. ISPRS Journal of Photogrametry and Remote Sensing, 60, 315-322.

Gloux, B. (1984): Méthode acoustiques et informatiques appliquées à la cartographie rapide et détaillée des herbiers. *In* International Workshop on Posidonia oceanica Beds. Boudouresque, C.-F., Jeudy de Grissac, A. and Olivier, J. (eds), pp. 45-48, GIS Posidonie Press, Marseille.

Green, R. H. (1979): Sampling design and statistical methods for environmental biologists. John Wiley & Sons, New York, 257 pp

Gujja, B. and Finger-Stich A. (1996): What price prawn? Shrimp aquaculture's impact in Asia. Environment, 38, 12-39.

Hashim, M., Misbari, S., Yahya, N. N., Ahmad, S., Reba, M. N. and Komatsu, T. (2014). An approach for quantification of submerged seagrass biomass in shallow turbid coastal waters. In Geoscience and Remote Sensing Symposium (IGARSS), 2014 IEEE International. pp. 4439-4442, IEEE.

Hashimoto, T. and Nishimura, M. (1953): Sounding of artificial schools, rocks and sea plants fields by fish finder. Technical Report of Fishing Boat Laboratory, 4, 138-142 (in Japanese).

Hashimoto, T. and Nishimura, M. (1953): Study on detection of Japanese tang field by the ultrasonic fish-finder. Technical Report of Fishing Boat Laboratory, 5, 187-194 (in Japanese).

Hatakeyama, Y. and Maniwa, Y. (1978): On the investigation of seaweed distribution by utilizing the fish finder. Technical Report of Fishing Boat Laboratory, 73, 155-168 (in Japanese).

Huitric, M., Folke, C. and Kautsky, N. (2002): Development and government policies of the shrimp farming industry in Thailand in relation to mangrove ecosystems. Ecological Economics, 40, 441-455.

Jerlov, N.G. (1968): Optical oceanography. Elsevier, New York, 194 pp.

Jeudy de Grissac, A. and Boudoureque, C.-F. (1985): Rôle des herbiers de Phanérogames marines dans les mouvements des sédiments côtiers: les herbiers à Posidonia oceanica. In Acte du colloque pluridisciplinaire franco-japonais d'Océanographie Fiscicule 1. Ceccaldi, HJ. and Champalbert, G. (eds), pp.143-151, Société Franco-japonaise d'Océanographie, Marseille.

Kirkman, H. (1990): Seagrass distribution and mapping. In Seagrass research methods. Phillips, RC. and McRoy, CP (eds), pp.19-25, Monographs on oceanographic methodology, UNESCO, Paris.

Kitoh, H. (1983): Seaweed beds research by a scientific echosounder. Seikai Regional Fisheries Research Institute News, 43, 2-4 (in Japanese).

Komatsu, T. (1989): Day-night reversion in the horizontal distributions of dissolved oxygen content and pH in a *Sargassum* forest, Journal of Oceanographical Society of Japan, 45, 106-115.

Komatsu, T. (1996): Influence of a *Zostera* bed on the spatial distribution of water flow over a broad geographical area, In Seagrass biology: Proceedings of an international workshop Rottnest Island, Western Australia, 25-29 January 1996. Kuo, J, Phillips, RC, Walker DI. and Kirkman, H (eds), pp. 111-116, , Faculty of Science, The University of Western Australia, Nedlands.

Komatsu, T. (1997): Long-term changes in the *Zostera* bed area in the Seto Inland Sea (Japan), especially along the coast of the Okayama Prefecture. Oceanologica Acta, 20, 209-216.

Komatsu, T., Igarashi, C., Tatsukawa, K., Nakaoka, M., Hiraishi, T. and Taira, A. (2002a): Mapping of seagrass and seaweed beds using hydro-acoustic methods. Fisheries Science, 68, sup. I, 580-583.

Komatsu, T., Igarashi, C., Tatsukawa, K., Sultana, S., Matsuoka, Y. and Harada, S. (2003a): Use of multi-beam sonar to map seagrass beds in Otsuchi Bay, on the Sanriku Coast of Japan. Aquatic Living Resources, 16, 223-230.

Komatsu, T., Ishida, K., Iizumi, H., Okamoto, M. and Belsher, T. (2001): Utilization of ALOS data for mapping coastal ecosystem and managing fisheries activity, Proceeding 1st ALOS PI workshop, 384-386.

Komatsu, T., Takahashi, M., K. Ishida, K., Suzuki, T. and Tameishi, H. (2002b): Mapping aquaculture facilities in Yamada Bay in Sanriku Coast, Japan, by IKONOS satellite imagery. Fisheries Science, 68, sup. I, 584-587.

Komatsu, T. and Tatsukawa, T. (1998): Mapping of *Zostera marina* L. beds in Ajino Bay, Seto Inland Sea, Japan, by using echo-sounder and global positioning systems. Journal de Recherche Océanographique, 23, 39-46.

Komatsu, T., Tatsukawa, K., Ishida, K., Igarashi, C., Sultana, S., Takahashi, M. and Matsuoka, Y. (2002c): Development of methods mapping coastal zone along Sanriku Coast using satellite imagery and acoustic survey. *In* Conserving our coastal environment: man and the ocean. UNU-ORI-Iwate Symposium Marine Ecology and Environment, United Nations University, pp.33-47, Tokyo, Japan.

Komatsu, T., Mikami, A., Sultana, S., Ishida, K., Hiraishi, T. and Tatsukawa, K. (2003b): Hydro-acoustic methods as a practical tool for cartography of seagrass beds. Otsuchi Marine Science, 28, 72-79.

Komatsu, T. and H. Yamano (2000): Influence of seagrass vegetation on bottom topography and sediment distribution on a small spatial scale in the Dravuni Island Lagoon, Fiji. Biologia Marina Mediterranea, 7, 243-246.

Lathrop, R. G.. Montesano, P. and Haag, S. (2006) A multi-scale segmentation approach to mapping seagrass habitats using. Photogrammetric Engineering & Remote Sensing, 72, 665–675.

Lee Long, W.J., Mckenzie, L.J., Rasheed, M.A. and Coles, R.G. (1996): Monitoring seagrasses in tropical ports and harbours. In Seagrass biology: Proceedings of an international workshop Rottnest Island, Western Australia, 25-29 January 1996. Kuo, J, Phillips, RC, Walker DI. and Kirkman, H (eds), pp. 345-350, Faculty of Science, The University of Western Australia, Nedlands.

Lefèvre, J.R., Meinesz, A. and Gloux, B. (1984): Premières données sur la comparaison de trois méthôdes de cartographie des biocénoses marines. Rapports et procès-verbaux des réunions Commission Internationale pour L'Exploration Scientifique de la Mer Méditerranée, 29, 209-211.

Long, B.G., Skews, I.D. and Pointer, I.R. (1994): An efficient method for estimating seagrass biomass. Aquatic Botany, 47, 277-292.

Lyzenga, D.R. (1978): Passive remote-sensing techniques for mapping water depth and bottom features.

Applied Optics, 17, 379-383.

Lyzenga, D.R. (1981): Remote sensing of bottom reflectance and water attenuation parameters in shallow water using aircraft and Landsat data. International Journal of Remote Sensing, 10, 53-69.

Ma, Z. and Redmond, R.L. (1995): Tau coefficients for accuracy assessment of classification of remote sensing data. Photogrammetric Engineering and Remote Sensing, 61, 435-439.

McKenzie, L.J. (2003): Guidelines for the rapid assessment and mapping of tropical seagrass habitats. QFS, NFC, Cairns, 46pp.

Meinesz, A. (1997): Balisage de la limite inférieure de l'herbier de *Posidonia oceanica* en rade de Villefranche-sur-Mer (Alpes-Maritimes, France). Rapports et procès-verbaux des réunions Commission Internationale pour L'Exploration Scientifique de la Mer Méditerranée, 24, 143-144.

Meinesz, A., and Laurent, R. (1978): Cartographie et état de la limite inférieure de l'herbier de *Posidonia oceanica* dans les Alpes-maritimes (France) -Campagne Poseidon 1976-. Botanica Marina, 21, 513-526.

Meinesz, A. Cuvelier, M. and Laurent, R. (1981): Méthode récentes de cartographie et de surveillance des herviers de Phanérogames marines. Vie et Milieu, 31, 27-34.

Meinesz, A., Boudouresque, C-F. and Lefèvre, J.R. 1988. A map of the *Posidonia oceanica* beds of Marina d'Elbu (Corsica, Mediterranean). P.S.Z.N.: Marine Ecology, 9, 243-252.

Mellors, J. E. (1991): An evaluation of a rapid visual technique for estimating seagrass biomass. Aquatic Botany, 42(1), 67-73.

Mumby, P. J., Clark, C.D., Green, E.P. and Edwards, A.J. (1998): Benefits of water column correction and contextual editing for mapping coral reefs. International Journal of Remote Sensing, 19, 203–210.

Mumby, P. J., Edwards, A. J., Green, E. P., Anderson, C. W., Ellis, A. C. and Clark, C. D. (1997a). A visual assessment technique for estimating seagrass standing crop. Aquatic Conservation: Marine and Freshwater Ecosystems, 7(3), 239-251.

Mumby, P. J., Green, E. P., Edwards, A. J. and Clark, C. D. (1997b): Measurement of seagrass standing crop using satellite and digital airborne remote sensing. Marine Ecology Progress Series, 159, 51-60.

Mumby, P. J., Green, E. P., Edwards, A. J. and Clark, C. D. (1999): The cost-effectiveness of remote sensing for tropical coastal resources assessment and management. Journal of Environmental Management, 55, 157–166

Naylor, R. L., Goldburg, R. J., Primavera, J. H., Kautsky, N., Beveridge, M. C., Clay, J., Folke, C., Lubchenco, J., Mooney H. and Troell, M. (2000): Effect of aquaculture on world fish supplies. Nature, 405(6790), 1017-1024.

Newton, R.S. and Stefanon, A. (1975): Application of side scan sonar in marine biology. Marine Biology, 31, 287-291.

Norris, J.G., Wyllie-Echeverria, S., Mumford, T., Bauley, A. and Turner, T. (1997): Estimating basal area coverage of subtidal seagrass beds using underwater videography. Aquatic Botany, 58, 269-287.

Orth, R.J., Heck, K.L.J. and Van Monfrans, J. (1984): Faunal communities in seagrass beds. A review of the

influence of plant structure and prey characteristics on predatory-prey relationships. Estuary, 7, 339-350.

Kuwahara, V. S., Toda, T., Hamasaki, K., Kikuchi, T. and Taguchi, S. (2000): Variability in the relative penetration of ultraviolet radiation to photosynthetically available radiation in temperate coastal waters, Japan. Journal of Oceanography, 56, 399-408.

Pasqualini, V. and Pergent-Martini, C. (1996): Monitoring of Posidonia oceanica meadows using image processing. In Seagrass biology: Proceedings of an international workshop Rottnest Island, Western Australia, 25-29 January 1996. Kuo, J, Phillips, RC, Walker, DI. and Kirkman, H (eds), pp. 351-358, Fac. Sci. Univ. West., Australia, Western Australia, Nedlands.

Pasqualini, V., Pergent-Martini, C., Clabaut, P. and Pergent, G. (1998): Mapping of Posidonia oceanica using aerial photographs and side scan sonar: Application off Island of Corsica (France). Estuarine, Coastal and Shelf Science, 47, 359-367.

Pasqualini, V., Pergent-Martini, C., Pergent, G., Agreil, M., Skoufas, G., Sourbes, L., and Tsirika, A. (2005): Use of SPOT 5 for mapping seagrasses: An application to *Posidonia oceanica*. Remote Sensing of Environment, 94, 39-45.

Ramos, M.A. and Ramos-Espla, A. (1989): Utilization of acoustic methods in the cartography of the *Posidonia oceanica* bed in the bay of Alicante (SE, Spain). Posidonia Newsletter, 2, 17-19.

Rey, J. and Diaz del Rio, V. (1989): Cartographia de los fondos marinos de la Bachia de Palma (Baleares, Espana): Distribution de las praderas vegetales y sedimentos superficiales. In International Workshop on Posidonia beds 2 GIS. Boudouresque, C-F., Meinesz, A., Fresi, E. and Gravez, V. (eds), pp. 29-41, Posidonie Press, Marseille.

Roelfsema, C., Kovacs, E. M., Saunders, M. I., Phinn, S., Lyons, M. and Maxwell, P. (2013): Challenges of remote sensing for quantifying changes in large complex seagrass environments. Estuarine, Coastal and Shelf Science, 133 161-171.

Sagawa, T., Mikami, A., Komatsu, T., Kosaka, N., Kosako, A., Miyazaki, S. and Takahashi, M. (2008): Mapping seagrass beds using IKONOS satellite image and side scan sonar measurements: a Japanese case study. International Journal of Remote Sensing, 29, 281–291.

Sagawa, T., Boisnier, E. Komatsu, T., Ben Mustapha, K., Hattour, A., Kosaka, N. and Miyazaki, S. (2010): Using bottom surface reflectance to map coastal marine areas: a new application method for Lyzenga's model. International Journal of Remote Sensing, 31, 3051–3064

Short, F. and Willie-Echeverria, S. (1996): Natural and human-induced disturbance of seagrasses. Environmental Conservation, 23, 17-27.

Tanaka, M. and Tanaka, K. (1985): On the estimation of the abundance of seaweed in coastal area I, estimation by echosounder. Fisheries Civil Engineering, 21, 17-23 (in Japanese).

Tanre, D., Deroo, C., Duhaut, P., Herman, M., Morcrette, J. J., Perbos, J. and Deschamps, P. Y. (1990): Description of a computer code to simulate the satellite signal in the solar spectrum: 5S code. International Journal of Remote Sensing, 11, 659–668.

Taylor, M. (2005): IKONOS planetary reflectance and mean solar exoatmospheric irradiance, IKONOS planetary reflectance QSOL Rev.1. Available online at: http://www.geoeye.com/products/imagery/ikonos/spectral.htm (accessed 15 January 2015).

Urbański, J. A., Mazur, A. and Janas, U. (2010): Object-oriented classification of Quickbird data for mapping seagrass spatial structure. International Journal of Oceanography and Hydrobiology, 38, 27–43.

USGS (2014): Using the USGS Landsat 8 Product. Available online at: http://landsat.usgs.gov/Landsat8_Using_Product.php (accessed 15 December 2014).

Vermote, E., Tanre, D., Deuze, J. L., Herman, M. and Morcrette, J. J. (1997): Second simulation of the satellite signal in the solar spectrum, 6S: An overview, IEEE Transaction on Geoscience and Remote Sensing, 35, 675-686.

Ward, L.G., Kemp, W.M. and Boyton, W.R. (1984): The influence of waves and seagrass communities on suspended particulates in an estuarine embayment. Marine Geology, 59, 85-103.

Xiaohe, Z., Z. Liang, Z. Jixian and S. Huiyong (2014) An object-oriented classification method of high resolution imagery based on improved AdaTree. IOP Conference Series: Earth and Environmental Science, 17, 012212. doi:10.1088/1755-1315/17/1/012212